3-30-2009

Scanning tunneling microscopy on epitaxial bilayer graphene on ruthenium (0001)

Eli A. Sutter
University of Nebraska–Lincoln, esutter@unl.edu

D.P. Acharya
Brookhaven National Laboratory

J.T. Sadowski
Brookhaven National Laboratory

P. Sutter
Brookhaven National Laboratory, psutter@unl.edu

Scanning tunneling microscopy on epitaxial bilayer graphene on ruthenium (0001)

E. Sutter, D. P. Acharya, J. T. Sadowski, and P. Sutter[a)]
Center for Functional Nanomaterials, Brookhaven National Laboratory, Upton, New York 11973, USA

(Received 5 January 2009; accepted 4 February 2009; published online 30 March 2009)

The atomic structure of epitaxial single and bilayer graphene on Ru(0001) was studied by scanning tunneling microscopy (STM). High-resolution imaging of the surface of single layer graphene shows a moiré with pronounced buckling and broken A/B carbon sublayer symmetry due to a strong interaction with the metal substrate. The top sheet of bilayer graphene is largely unperturbed by residual interactions with the substrate. Screened from the metal substrate, it shows the hallmarks of freestanding monolayer graphene: a honeycomb structure with equivalent carbon sublattices imaged in STM and a linear dispersion of π-bands near the Dirac point. © *2009 American Institute of Physics*. [DOI: 10.1063/1.3106057]

Graphene, a two-dimensional honeycomb lattice of sp^2 bonded carbon atoms,[1] has shown a number of remarkable properties that make it a promising material for large-scale applications in microelectronics[2,3] and sensing.[4] To realize this potential, reliable methods for fabricating large-area single crystalline graphene domains are required. Graphene synthesis by epitaxy on noncarbide-forming transition metals[5,6] has been considered recently as a promising alternative to micromechanical cleavage for producing macroscopic graphene domains. On the (0001) surface of ruthenium (Ru), in particular, it has been shown that one can produce large (close to 500 μm) single or bilayer epitaxial graphene nuclei in a controlled layer-by-layer fashion.[5] Graphene interacts strongly with Ru. Thus a single graphene layer has a significantly altered electronic structure compared to freestanding graphene and an atomic structure reflecting the strong substrate coupling.[5,7] While much effort has been invested in determining the properties of monolayer graphene (MLG) on Ru(0001),[7–9] the atomic structure of bilayer epitaxial graphene has not been investigated yet.

The possibility of controlled growth of bilayer graphene (BLG) domains on Ru(0001) raises several important issues, which can be addressed by high-resolution microscopy. While Raman spectroscopy suggests that the top sheet in BLG on Ru(0001) recovers the electronic structure of freestanding MLG,[5] it is unclear if the sheet is homogeneously decoupled from the first layer and substrate. Further, many of the exotic electronic properties of graphene derive from the chiral nature of its Dirac fermions,[2,10] originating in the two-atom basis (i.e., A and B sublattices) of the honeycomb structure of graphene. Thus, it needs to be verified if the A and B carbon sublattices of the top sheet of the bilayer are equivalent (i.e., the charge carriers chiral) or if the underlying buffer breaks the sublattice symmetry (leading to nonchiral carriers). Local spectroscopy, finally, can be used to establish the residual charge-transfer doping of the bilayer by determining the energy of the Dirac point, i.e., the crossing of the linear π-bands at the K-point of the two-dimensional Brillouin zone.

Here, we address these issues by scanning tunneling microscopy (STM) imaging and spectroscopy of single and bilayer epitaxial graphene on Ru(0001). The study is based on the ability to grow macroscopic epitaxial graphene sheets with predictable thickness in a controlled layer-by-layer mode on Ru. The graphene growth was carried out in a preparation chamber attached to an ultrahigh vacuum (UHV) STM following the procedure described in Ref. 5. Briefly, a clean Ru(0001) single crystal was loaded with interstitial carbon by exposure to a hydrocarbon precursor (ethylene) at high temperature (>1000 °C). Graphene was grown in UHV by slowly lowering the sample temperature, driving the controlled segregation of C to the Ru surface. The graphene growth proceeds via the initial formation of monolayer thick graphene islands that expand to a size corresponding to the spacing of the initial nuclei and coalesce to a complete graphene monolayer covering the entire Ru(0001) substrate. Upon completion of the first layer, a second graphene layer nucleates and can again grow to domain sizes of over 100 μm if the slow temperature ramp is continued. STM imaging and spectroscopy on samples with full monolayer coverage and with additional small second layer nuclei was performed *in situ* using a Createc low-temperature STM cooled to 77 K. The STM measurements were complemented by selected-area angle-resolved photoemission spectroscopy (micro-ARPES), performed *in situ* at 300 K on individual larger BLG domains in a Elmitec LEEM III low-energy electron microscope with energy analyzer (energy resolution ~200 meV), using 42 eV synchrotron radiation.

On Ru(0001), single layer graphene adopts a moiré structure[5,7,8] in which the $\langle 10\bar{1}0\rangle$ directions of layer and substrate align, with moiré repeat vectors $a_m = 2.93 \pm 0.08$ nm, equivalent to 10.8 ± 0.3 times the nearest-neighbor distance on Ru(0001).[5] Figure 1(a) is an overview STM image of this moiré structure. The graphene monolayer shows large variations in apparent height (about 1 Å) within a highly ordered moiré structure that has no visible defects over very large sample areas. High-resolution STM images [Fig. 1(b)] show no atomic-scale defects, indicating a high crystalline quality of the graphene layer. Superimposed over the large long-range height variations is a mostly triangular lattice structure at the atomic scale, similar to the one observed earlier[7] and

[a)]Author to whom correspondence should be addressed. Electronic mail: psutter@bnl.gov.

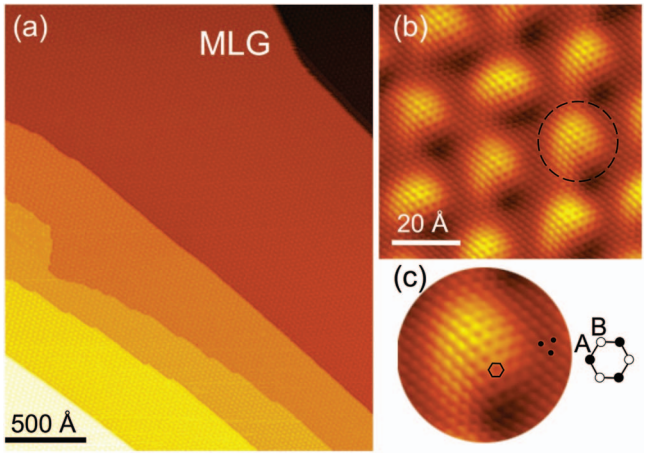

FIG. 1. (Color) Morphology of first-layer epitaxial graphene on Ru(0001). (a) UHV STM image, obtained at 77 K, of a large area of monolayer epitaxial graphene on Ru(0001). (b) High-resolution STM image of the moiré structure of the graphene layer ($V=+0.2$ V, $I=0.2$ nA). (c) Magnified view of the highest region of the moiré, showing a local honeycomb structure.

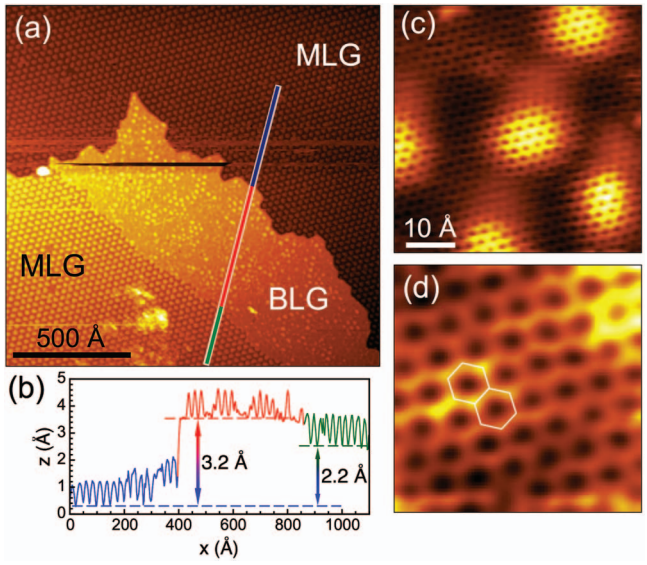

FIG. 2. (Color) Morphology of the top sheet of bilayer epitaxial graphene on Ru(0001). (a) UHV STM image ($T=77$ K) of the surface consisting of two different phases: a BLG island on a completed MLG layer. (b) Height profile along the line displayed in a. (c) High-resolution STM image showing honeycomb contrast, i.e., sublattice equivalency, in rippled and flat regions of the bilayer. (d) Closeup view of the graphene honeycomb lattice ($V=+0.7$ V, $I=0.2$ nA).

assigned to a moiré pattern whose atomic contrast varies across the unit cell depending on the local registry with the surface Ru atoms. The local registry determines which of the graphene *A* or *B* sublattices is imaged. In most parts of the moiré unit cell the sublattice symmetry is broken and only one of the two carbon sublattices is imaged due to the strong, covalent interaction with the substrate. The full graphene honeycomb lattice is only visible in areas directly adjacent to the moiré maxima [Fig. 1(c)]. In these regions the graphene sheet is lifted higher above the Ru lattice and couples weakly to it.[9] As a result, the density of states (DOS) of the two sublattices is identical in these areas and the full honeycomb of both *A* and *B* carbon atoms is imaged by STM.

While the atomic structure of the graphene monolayer shown in Fig. 1 is dominated by the strong covalent interaction with the metal substrate, it is important to establish the surface structure of the graphene bilayer, whose topmost sheet is expected to be almost completely decoupled and only interacting with the support via weak van der Waals forces.[5] In order to ensure the unambiguous identification of the bilayer, the growth was modified to yield only small nuclei of the second graphene layer. This was achieved by growing the monolayer to saturation coverage, and then rapidly lowering the sample temperature.

Figure 2(a) shows a typical BLG island and the surrounding completed monolayer. The island is bounded on one side by a Ru surface step and on the other by a kinked but atomically sharp edge whose segments align with the major crystallographic directions of the underlying moiré structure of the monolayer. The surface of the bilayer island shows distinct inhomogeneous STM contrast that appears less ordered than the surrounding monolayer areas. While a majority of the sheet is flat, it also carries surface ripples of varying height, the highest of which protrude about 1 Å. In the sample plane, the positioning of these ripples shows no long-range order. In some areas the ripples are in a local hexagonal arrangement with the periodicity and orientation of the superstructure of the adjacent monolayer but they generally do not align with the maxima of the monolayer moiré.

Figure 2(b), a profile of apparent height in STM along the line traced in Fig. 2(a), shows a height difference of ~2.2 Å between two terraces entirely covered by MLG, corresponding to the interlayer spacing of the (0001)-oriented Ru (2.14 Å). These areas covered by MLG are thus grown on adjacent substrate terraces and separated by an atomic Ru step. Although the contrast in STM invariably reflects a combination of topographic and electronic structure and can be difficult to interpret on inhomogeneous surfaces, the measured height difference between the two sheets of the bilayer (3.2 Å, relative to the monolayer minima) is close to the *c*-axis spacing of graphite (3.35 Å), as expected if the top sheet of the bilayer is coupled to the underlying support by weak van der Waals forces only.

The equivalence of *A* and *B* carbon sublattices in graphene requires a description of electronic Bloch states in terms of two component wave functions and gives rise to exciting phenomena such as chiral quantum Hall effects[2,10] and anisotropic group velocity renormalization[11] and electron supercollimation[12] in lateral superlattices. It is therefore important to establish if the decoupling of top sheet of epitaxial BLG on Ru is sufficient to recover the A/B sublattice symmetry. This question can be addressed by high-resolution STM. Atomically resolved images [Figs. 2(c) and 2(d)] obtained on the bilayer show symmetrical honeycomb contrast throughout, i.e., in both planar and rippled areas. The honeycomb structure is characteristic of a single graphene layer for which all carbon atoms are equivalent and has been observed by STM on cleaved MLG on SiO_2.[13,14] The atomic structure observed here shows that the top sheet in bilayer epitaxial graphene on Ru(0001) is weakly perturbed by residual support interactions and has the characteristics of freestanding MLG. In particular its carbon sublattices are equivalent so that its charge carriers should behave as massless and chiral Dirac fermions, showing the rich behavior observed or predicted for such charge carriers in isolated MLG.

To further explore the electronic decoupling of the top sheet of epitaxial BLG, we have performed scanning tunnel-

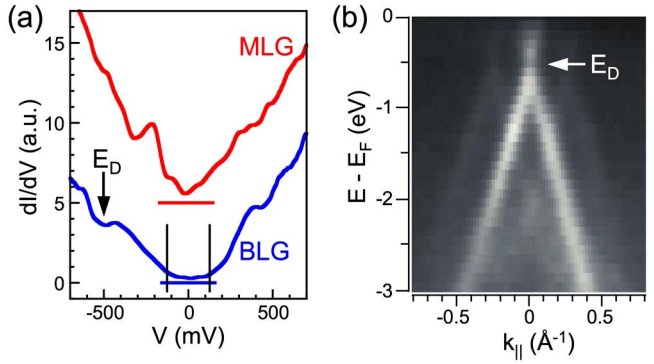

FIG. 3. (Color online) Electronic structure of the top sheet of bilayer epitaxial graphene on Ru(0001). (a) dI/dV tunneling spectra of MLG and BLG domains. Horizontal lines mark $dI/dV=0$; vertical lines denote energies $\pm\hbar\omega_0$ of the K_2 acoustic phonon (Ref. 16). (b) Micro-ARPES spectrum on BLG, obtained near the K-point of the Brillouin zone in a direction perpendicular to $\overline{\Gamma\text{-K}}$.

ing spectroscopy on both monolayer and bilayer domains. Representative local dI/dV spectra are shown in Fig. 3(a). The spectrum of the monolayer shows pronounced modulations of the tunneling conductance near the Fermi energy (E_F), reflecting the DOS of a graphene sheet strongly interacting with the metal substrate. The state at about -0.2 eV, for instance, is also observed in micro-ARPES spectra at small in-plane momentum on the monolayer.[15] From a minimum at E_F, dI/dV increases sharply with energy for both filled and empty states, consistent with a finite DOS at E_F near the zone center. The situation is different for the bilayer. Here, the tunneling conductance remains close to zero within an extended energy window around E_F. A similar gaplike feature observed in tunneling spectra on exfoliated graphene/SiO_2 (Ref. 14) was interpreted as due to a suppression in elastic tunneling close to E_F, followed by a sharp rise in the tunneling conductance with the onset of inelastic tunneling involving the emission of a K_6 acoustic phonon with energy $\hbar\omega_0 \approx 67$ meV.[16] For BLG on Ru(0001), however, the gap is significantly wider. If the tunneling indeed is due to the opening of an inelastic channel at the energy of a K-point acoustic phonon, our data suggest that the excitation of the lowest-energy out-of-plane K_6 phonon mode is suppressed, and that the gap is instead defined by the in-plane K_2 phonon with $\hbar\omega_0 \approx 125$ meV.[16] At higher negative bias, the tunneling spectrum of BLG on Ru(0001) is similar to electron-doped MLG SiO_2, which showed a pronounced dip in dI/dV at the Dirac energy, i.e., the energy at which the linear π-bands intersect.[14] Adopting the same interpretation for our spectra, we would place the Dirac energy at $E_D \approx -500$ meV, consistent with a substantial electron doping of the decoupled top sheet of the bilayer by the underlying graphene buffer and metal substrate. Micro-ARPES spectra on larger BLG domains on Ru(0001) indeed show a linear band dispersion near K, with Dirac point about 500 meV below E_F [Fig. 3(b)], confirming that the top sheet of the bilayer behaves like freestanding MLG except for a downshift of the Dirac point. Our STM and initial micro-ARPES results suggest that the decoupling of the top sheet of the bilayer is due to a suppression of π-states of the bottom layer by hybridization with Ru d-states. Such a process would leave only the π-states of an isolated top layer near E_F at the K-point.

In conclusion, we have established the atomic and electronic structure of bilayer epitaxial graphene on Ru(0001). The interfacial graphene sheet in the bilayer plays the role of a buffer, coupling strongly to the metal and screening the top sheet from the metal d-states. As a result, the top sheet of the bilayer recovers the structure (a symmetric honeycomb lattice) and electronic properties (linear dispersion in Dirac cones) of freestanding MLG.

Work performed under the auspices of the U.S. Department of Energy under Grant No. DE-AC02-98CH1-886.

[1] A. K. Geim and K. S. Novoselov, Nature Mater. **6**, 183 (2007).
[2] K. S. Novoselov, A. K. Geim, S. V. Morozov, D. Jiang, M. I. Katsnelson, I. V. Grigorieva, S. V. Dubonos, and A. A. Firsov, Nature (London) **438**, 197 (2005).
[3] S. V. Morozov, K. S. Novoselov, M. I. Katsnelson, F. Schedin, D. C. Elias, J. A. Jaszczak, and A. K. Geim, Phys. Rev. Lett. **100**, 016602 (2008).
[4] F. Schedin, A. K. Geim, S. V. Morozov, E. W. Hill, P. Blake, M. I. Katsnelson, and K. S. Novoselov, Nature Mater. **6**, 652 (2007).
[5] P. W. Sutter, J.-I. Flege, and E. A. Sutter, Nature Mater. **7**, 406 (2008).
[6] A. T. N'Diaye, S. Bleikamp, P. J. Feibelman, and T. Michely, Phys. Rev. Lett. **97**, 215501 (2006).
[7] S. Marchini, S. Gunther, and J. Wintterlin, Phys. Rev. B **76**, 075429 (2007).
[8] A. L. Vazquez de Parga, F. Calleja, B. Borca, M. C. G. Passeggi, Jr., J. J. Hinarejo, F. Guinea, and R. Miranda, Phys. Rev. Lett. **100**, 056807 (2008).
[9] B. Wang, M.-L. Bocquet, S. Marchini, S. Günther, and J. Wintterlin, Phys. Chem. Chem. Phys. **10**, 3530 (2008).
[10] Y. Zhang, J. W. Tan, H. L. Stormer, and P. Kim, Nature (London) **438**, 201 (2005).
[11] C.-H. Park, L. Yang, Y.-W. Son, M. L. Cohen, and S. G. Louie, Nat. Phys. **4**, 213 (2008).
[12] C.-H. Park, Y.-W. Son, L. Yang, M. L. Cohen, and S. G. Louie, Nano Lett. **8**, 2920 (2008).
[13] E. Stolyarova, K. T. Rim, S. Ryu, J. Maultzsch, P. Kim, L. E. Brus, T. F. Heinz, M. S. Hybertsen, and G. W. Flynn, Proc. Natl. Acad. Sci. U.S.A. **104**, 9209 (2007).
[14] Y. Zhang, V. W. Brar, F. Wang, C. Girit, Y. Yayon, M. Panlasigui, A. Zettl, and M. F. Crommie, Nat. Phys. **4**, 627 (2008).
[15] P. Sutter, J. T. Sadowski, M. S. Hybertsen, and E. Sutter (unpublished).
[16] M. Mohr, J. Maultzsch, E. Dobardzic, S. Reich, I. Milosevic, M. Damnjanovic, A. Bosak, M. Krisch, and C. Thomsen, Phys. Rev. B **76**, 035439 (2007).